Combining OCT and OCTA for Focal Structure–Function Modeling in Early Primary Open-Angle Glaucoma

Damon Wong,[1–3] Jacqueline Chua,[3,4] Bingyao Tan,[1–3] Xinwen Yao,[1–3] Rachel Chong,[3] Chelvin C. A. Sng,[3,5] Rahat Husain,[3] Tin Aung,[3–6] David Garway-Heath,[7,8] and Leopold Schmetterer[1–3,5,9–11]

[1]SERI-NTU Advanced Ocular Engineering (STANCE), Singapore
[2]School of Chemical and Biomedical Engineering, Nanyang Technological University, Singapore
[3]Singapore Eye Research Institute, Singapore National Eye Centre, Singapore
[4]Academic Clinical Program, Duke-NUS Medical School, Singapore
[5]Department of Ophthalmology, National University Hospital, Singapore
[6]Department of Ophthalmology, National University Hospital, Singapore
[7]NIHR Biomedical Research Centre at Moorfields Eye Hospital NHS Foundation Trust, London, United Kingdom
[8]Institute of Ophthalmology, University College, London, United Kingdom
[9]Department of Clinical Pharmacology, Medical University of Vienna, Vienna, Austria
[10]Center for Medical Physics and Biomedical Engineering, Medical University of Vienna, Vienna, Austria
[11]Institute of Molecular and Clinical Ophthalmology, Basel, Switzerland

Correspondence: Leopold Schmetterer, Singapore Eye Research Institute, 20 College Road, The Academia, Level 6, Discovery Tower, 169856, Singapore; leopold.schmetterer@seri.com.sg.

Received: July 22, 2021
Accepted: November 12, 2021
Published: December 8, 2021

Citation: Wong D, Chua J, Tan B, et al. Combining OCT and OCTA for focal structure–function modeling in early primary open-angle glaucoma. *Invest Ophthalmol Vis Sci.* 2021;62(15):8. https://doi.org/10.1167/iovs.62.15.8

Purpose. To investigate modeling of the focal visual field (VF) loss by combining structural measurements and vascular measurements in eyes with early primary open-angle glaucoma (POAG).

Methods. In this cross-sectional study, subjects with early glaucoma (VF mean deviation, ≥−6 dB) underwent optical coherence tomography (OCT) imaging, optical coherence tomography angiography (OCTA) imaging, and Humphrey 24-2 VF tests. Capillary perfusion densities (CPDs) were calculated after the removal of large vessels in the OCTA images. Focal associations between VF losses at the individual VF test locations, circumpapillary retinal nerve fiber layer (RNFL) thickness measurements from OCT, and CPDs were determined using nerve fiber trajectory tracings. Linear mixed models were used to model focal VF losses at each VF test location.

Results. Ninety-seven eyes with early POAG (VF mean deviation, −2.47 ± 1.64 dB) of 71 subjects were included. Focal VF modeling using a combined RNFL–CPD approach resulted in a median adjusted R^2 value of 0.30 (interquartile range [IQR], 0.13–0.55), whereas the RNFL-only and CPD-only approaches resulted in median values of 0.22 (IQR, 0.10–0.51) and 0.26 (IQR, 0.10–0.52), respectively. Seventeen VF locations with the combined approach had an adjusted R^2 value greater than 0.50. Likelihood testing at each VF test location showed that the combined approach performed significantly better at the superior nasal VF regions of the eyes compared with the univariate approaches.

Conclusions. Modeling of focal VF losses showed improvements when structural thickness and vascular parameters were included in tandem. Evaluation of VF defects in early glaucoma may benefit from considering both RNFL and OCTA characteristics.

Keywords: structure–function, visual field, OCT, OCTA, focal

Glaucoma is an optic neuropathy characterized by the progressive loss of retinal ganglion cells and their axons and the gradual loss of vision. Clinical detection and monitoring of glaucoma are performed by assessment of functional vision loss using standard automated perimetry[1] and measurement of structural changes in the retinal nerve fiber layer (RNFL) thickness using optical coherence tomography (OCT).[2,3] Reduced ocular perfusion has also been associated with glaucoma,[4–7] and there are indicators that vascular factors play a role in disease pathogenesis.[8,9] OCT angiography (OCTA) is a recent technique[10,11] for the visualization of retinal perfusion to the level of capillaries.[12] In glaucoma, the usefulness of OCTA-based vascular metrics has been demonstrated in the discrimination of diseased eyes from healthy eyes.[13–15] Relating structural and, increasingly, vascular[16–25] changes with functional loss of vision in glaucoma is referred to as the structure–function relationship.[26–28]

Various studies have been conducted to investigate a more spatially specific focal structure–function relationship, including determining changes based on hemifields[20,29,30] and region-based associations[14,17,22,31–34] using the

Garway–Heath map,[35] as well as, more recently, focal correlations[16] at individual visual field (VF) locations using nerve fiber trajectory tracings.[36,37] These studies have largely shown that vascular parameters are less susceptible to floor effects in subjects with more severe VF losses compared with RNFL thickness measurements.[16,32,38] However, the majority of these studies investigated the structure–function relationship with RNFL or vascular measures separately, and there has been limited work investigating the combination of both, particularly in subjects with early glaucoma. The purpose of this study was to evaluate focal structure–function relationships using OCT RNFL thickness measurements and OCTA vascular parameters in a cohort of eyes with early primary open-angle glaucoma (POAG).

Methods

Study Population

This cross-sectional study was conducted at the Singapore National Eye Centre, a specialized eye care institution in Singapore. Study protocols adhered to the tenets of the Declaration of Helsinki and were approved by the SingHealth Centralized Institutional Review Board. Written informed consent was obtained from all participants. Subjects had clinically diagnosed POAG, based on eyes having a glaucomatous optic disc appearance not due to secondary causes of optic neuropathy (defined as loss of neuroretinal rim with a vertical cup-to-disc ratio of >0.7 or an inter-eye asymmetry of >0.2 and/or notching attributable to glaucoma) with compatible VF loss, a corresponding glaucoma hemifield test outside normal limits, and open angles on gonioscopy. Early glaucoma was staged based on VF mean deviation of ≥ -6 dB from standard automated perimetry using the simplified Bascom Palmer Glaucoma Staging System.[39]

Clinical Examinations

All participants received a standardized ophthalmic examination, which included assessment of VF acuity using a logarithm of minimum angle of resolution (logMAR) chart (Precision Vision, Woodstock, IL, USA), autorefractometry (Canon RK-5 Autorefractor Keratometer; Canon Inc., Tokyo, Japan), intraocular pressure measurement using Goldman applanation tonometry, VF assessment, OCT, and OCTA. Pupils were dilated with a drop of tropicamide 1% (Mydriacyl; Alcon, Geneva, Switzerland) prior to imaging. Refractive error was quantified based on the spherical equivalent (SE), defined as the spherical value plus half of the negative cylinder value. Eyes with SE ≤ -6D were excluded. VF assessment was performed using standard automated perimetry (Humphrey Field Analyzer; Carl Zeiss Meditec, Jena, Germany) with a 24-2 central threshold test using a Goldmann size III white stimulus and the Swedish interactive thresholding algorithm (SITA) Fast strategy. Only reliable VF tests with fixation losses less than 33%, false-positive errors less than 20%, and false-negative errors less than 20% were included.

OCT and OCTA Imaging

Subjects underwent OCT imaging with a spectral-domain OCT system (Cirrus 5000; Carl Zeiss Meditec) using a 200 × 200 optic nerve head scan protocol. The system works at 800-nm central wavelength with an A-scan rate of 70 kHz. Circumpapillary retinal nerve fiber layer thickness was obtained with a 3.46-mm-diameter circle centered on the optic nerve head from raster scan interpolations using an in-built protocol. OCTA imaging was performed using a prototype commercial swept-source OCT prototype (PLEX Elite 9000; Carl Zeiss Meditec), operating at an A-scan rate of 100 kHz with a central wavelength of 1040 nm to 1060 nm. En face OCTA images of the superficial capillary plexus were generated from the vertical projection of angiographic signals contained in the slab between the inner limiting membrane and the inner plexiform layer, using built-in software (PLEX Elite 9000 Review Software; Carl Zeiss Meditec) based on a microangiography technique.[40] Widefield macula-centered 12 mm × 12 mm and optic disc 6 mm × 6 mm scans were acquired. Images with signal strengths less than 6 and excessive movement artifacts were excluded. Regions of poor signal intensity that were observed in both OCT and OCTA images were manually excluded from subsequent analysis. Locations of the center of the optic disc, based on OCT, and the center of the macula, based on the center of the foveal avascular zone as determined on OCTA, were manually annotated and used to calculate the disc–fovea distance (DFD) and disc–fovea angle (DFA) for each eye.

Focal Structure–Function Modeling

Structure–function modeling was performed at each VF location based on nerve fiber trajectory tracing.[36,37] Details have been previously reported.[16] Briefly, a customized algorithm using MATLAB (MathWorks, Natick, MA, USA) was used to exclude large vessels and generate binarized capillary maps from the optic disc OCTA images. Nerve fiber trajectories adapted to the DFD and DFA of individual eyes were used to define focal regions associated with individual VF locations (Fig. 1). Specifically, the trajectories associated with each focal region defined the extents of the structural measurements based on the circumpapillary nerve fiber layer thickness (RNFL) from the OCT optic disc scan and the extents of the en face superficial vascular plexus from the corresponding OCTA optic disc scan. The mean RNFL thickness within the defined circumpapillary measurements and the capillary perfusion density (CPD) in the defined en face OCTA region were used as the focal structural RNFL and vascular CPD metrics, respectively.

Statistical Analysis

Demographic data are presented as mean (SD) and range where appropriate. VF sensitivities were converted to linear scale by taking the anti-log of the logarithmic decibel values.[41] Structure–function relationships were assessed with linear mixed-effect models to account for inter-eye correlations within the same subject. Models were compared using coefficient of variance (R^2) values, adjusted for the number of predictors in the model. Global characteristics were evaluated against VF mean deviation (VFMD). Focally, linear mixed model regression analysis was performed at each VF location with the associated focal CPD and focal RNFL metrics. Bivariate models using both CPD and RNFL included an interaction term to model interactions between the parameters. Comparisons of the bivariate models against the unimodal RNFL and CPD models at each VF location were assessed using likelihood-ratio testing. P values less

Investigative Ophthalmology & Visual Science

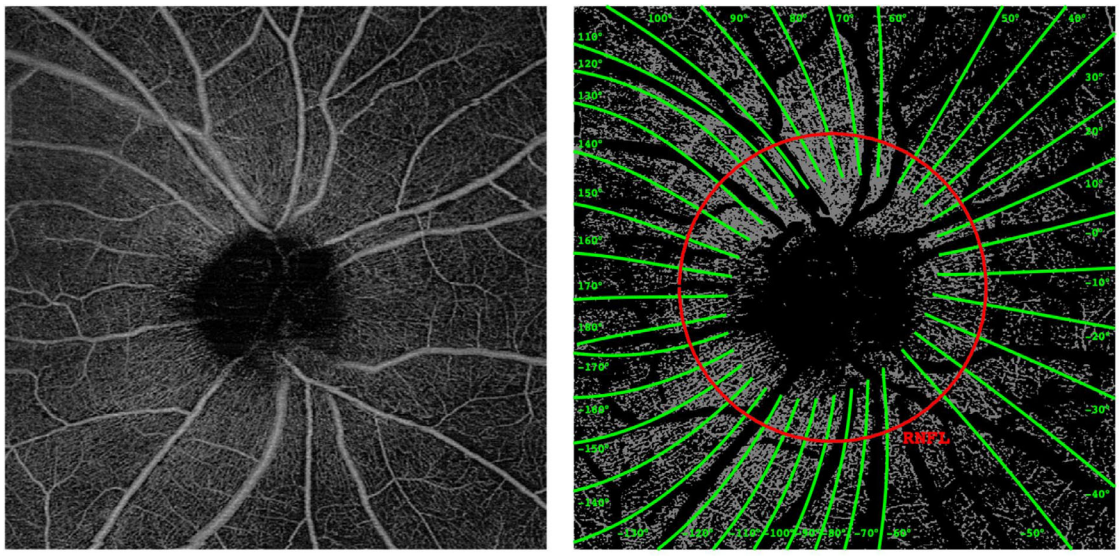

(C)

			-85 [-105,-60]	-84 [-103,-60]	-79 [-97,-60]	-67 [-85,-60]		
		-93 [-116,-61]	-98 [-119,-65]	-101 [-119,-86]	-99 [-113,-67]	-84 [-98,-60]	-60 [-74, -55]	
	-96 [-121,-65]	-104 [-129,-72]	-115 [-135,-81]	-124 [-137,-96]	-126 [-134,-110]	-111 [-116,-99]	-70 [-81, -60]	-55 [-60,-47]
-95 [-121,-66]	-103 [-131,-73]	-116 [-141,-82]	-132 [-150, -99]	-146 [-157,-126]	-155 [-160,-146]	-146 [-147,-144]		-45 [-55,-36]
109 [90,117]	112 [95,120]	116 [101,125]	124 [108,140]	151 [133,160]	163 [160,164]	159 [159,159]		-5 [-10,1]
	109 [87,117]	111 [91,120]	115 [96,127]	124 [99,137]	134 [102,138]	121 [94,124]	77 [67, 83]	41 [32,64]
		105 [80,115]	107 [81,117]	106 [81,118]	100 [76,114]	88 [67,100]	68 [60,78]	
			98 [68,111]	94 [65,108]	86 [60,101]	76 [60,90]		

Figure 1. Illustration of the focal structure–function map. (**A**) OCTA image of the superficial capillary plexus of a study eye. (**B**) Binarized capillaries with major vessels removed overlaid with nerve fiber trajectories indicated in *green*, with numbers indicating the angular coordinates based on the modified polar coordinate system developed by Jansonius and co-workers.[36,37] The *red circle* represents the scan pattern for the circumpapillary RNFL thickness measurement. The fiber trajectories are used to define the regions on the OCTA image for calculation of the focal CPD and arcs along the RNFL scan pattern for calculation of focal nerve fiber layer thickness. Further details on the implementation can be found in our previous publication.[16] (**C**) Mapping of the VF locations and associated trajectories.[36] Values indicate the mean and 95% confidence intervals of the angular coordinates for each VF location.

than 0.05 were considered to be statistically significant. Holm–Bonferroni corrections were used to adjust P values for multiple comparisons between models.[42] Statistical analyses were carried out using the commercial statistical software Stata 13.1 (StataCorp, College Station, TX, USA), and figures and visualizations were generated using MATLAB.

Results

Ninety-seven eyes from 71 Chinese subjects with early glaucoma (VFMD, -2.47 ± 1.64 dB) were included in the study. Subjects had a mean age of 63.5 ± 12.7 years with a mean refractive error of -1.26 ± 2.01 diopters (D). Characteristics of the participants are shown in Table 1, together with the corresponding univariate mixed model regression analyses. Global RNFL ($P = 0.001$; $R^2 = 0.481$) and global capillary density ($P = 0.007$; $R^2 = 0.428$) were the only parameters with significant coefficients in the univariate models. When both global RNFL and global capillary density were included, the combined model had an adjusted R^2 value of 0.649, and likelihood ratio testing showed that the combined model was significantly better than the univariate global RNFL ($P = 0.033$) and global capillary density ($P = 0.009$) models after performing Holm–Bonferroni correction.

A summary of the focal modeling of VF sensitivities across all of the VF locations is presented in Table 2 and Figure 2. Results of the performance of the different approaches at each VF location can be found in the Supplementary Table and Figure. Overall, the focal models using only RNFL achieved a median adjusted R^2 of 0.22 (interquartile range

Table 1. Demographic Characteristics of Study Subjects (97 Eyes, 71 Subjects)

Characteristics	Value	P^*	R^{2*}
Age (y), mean ± SD	63.5 ± 12.7	0.586	0.187
Gender (female:male), *n*	23:48	0.210	0.182
Refractive error (D), mean ± SD	−1.3 ± 2.0	0.810	0.144
Intraocular pressure (mmHg), mean ± SD	14.5 ± 2.8	0.420	0.193
Global RNFL thickness (µm), mean ± SD	75.3 ± 9.3	**0.001**	**0.481**
Global capillary density (%), mean ± SD	36.6 ± 7.2	**0.007**	**0.428**
Disc–fovea angle (°),† mean ± SD	9.4 ± 3.7	0.843	0.178
Disc–fovea distance (mm),‡ mean ± SD	4.5 ± 0.2	0.924	0.183
Signal strength, mean ± SD	8.5 ± 0.9	0.824	0.179
VF mean deviation (dB), mean ± SD	−2.5 ± 1.6	—	—

* Adjusted R^2 values are based on univariate linear mixed-effects modeling with VFMD. Characteristics with significant coefficients ($P < .05$) are in bold.

† Angle between the optic disc center and the foveola, with respect to the horizontal.

‡ Distance between the optic disc center and the foveola.

Table 2. Summary of Likelihood Ratio Test Results at Each Focal Location Comparing the Combined RNFL–CPD Model Against the Nested RNFL or CPD Model

Model†	Likelihood Ratio Test*	
	N_{LR}	$N_{LR,HB}$
Focal retinal nerve fiber thickness	18 (35.2%)	13 (25.4%)
Focal capillary density	12 (23.5%)	9 (17.6%)

* Summary of likelihood ratio tests comparing the combined RNFL–CPD model against the nested unimodal model. N_{LR} indicates the number of VF locations in which the combined model was significantly ($P < .05$) better; $N_{LR,BF}$ indicates the number of significant locations that were better after correcting with Holm–Bonferroni. Values in parentheses for N_{LR} and $N_{LR,HB}$ represent the number of VF test locations as a percentage of all test locations (51).

† Regression analysis was performed at each VF test location using focal RNFL, focal CPD, and a combined model with both focal RNFL and CPD. One VF test location at eccentricity (9°, −3°) was excluded due to the limited region of the focal nerve layer and CPD defined by the trajectories for that location.

[IQR], 0.10–0.51) and models using only CPD resulted in a median adjusted R^2 of 0.26 (IQR, 0.10–0.52). The combined RNFL–CPD models achieved a median adjusted R^2 of 0.30 (IQR, 0.13–0.55). For the combined models, 17 VF locations (33.0%) had adjusted R^2 values greater than 0.5, compared with 15 VF locations (29.4%) for the CPD-only models and 14 (27.5%) for the RNFL-only models. Likelihood ratio tests at each VF location comparing the combined models with the univariate models showed that the combined models were significantly better than the RNFL-only models at 13 VF locations (18 significant without Holm–Bonferroni correction) and the CPD-only models at nine VF locations (12 significant without Holm–Bonferroni correction). In total, there were 16 VF locations (23 significant without Holm–Bonferroni correction) in which the combined RNFL–CPD model was found to be significantly better than either RNFL or CPD models. The spatial distributions of the performance of the models with respect to the specific VF locations are presented in Figure 3. The combined model largely showed better performance for the VF locations in the superior nasal VF regions, after adjusting for Holm–Bonferroni.

Discussion

In this study, we found that combining RNFL thickness and vascular parameters resulted in better focal structure–function relationships than models with RNFL or vascular parameters alone in early POAG. Likelihood ratio comparisons at each VF test point showed that the RNFL–CPD

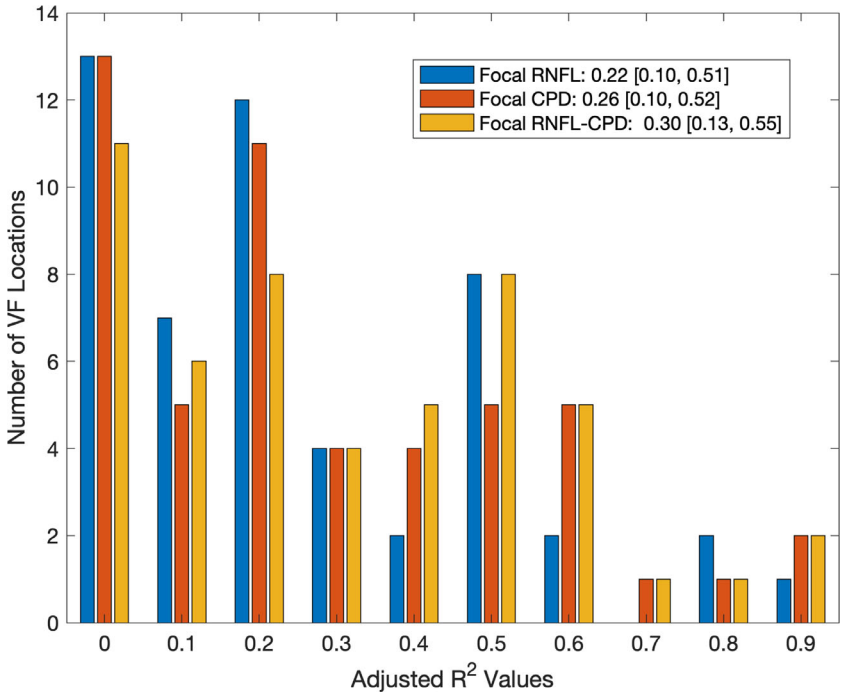

Figure 2. Distributions of the performance of the different approaches used to model focal VF loss from all VF test points. R^2 values were adjusted for the number of predictors in the model. Values in the legends indicate the median, with *square brackets* indicating the 25% and 75% quantiles for the corresponding model. Labels on the *x*-axis indicate the lower bounds of the histogram bins.

Investigative Ophthalmology & Visual Science

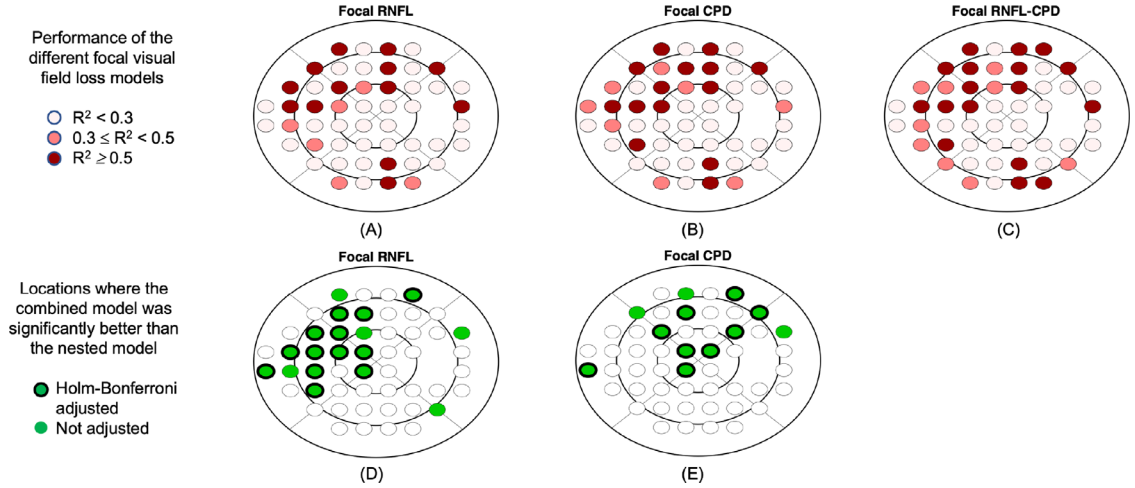

Figure 3. Spatial distributions of the results obtained from the focal structure–function models. The *top row* presents model performance in terms of adjusted R^2 values with respect to the individual focal VF locations for the (**A**) RNFL-only approach, (**B**) CPD-only approach, and (**C**) combined RNFL–CPD approach. The *second row* presents the results of the likelihood ratio tests comparing the combined RNFL–CPD model against the univariate (**D**) RNFL-only or (**E**) CPD-only models at individual VF locations. Holm–Bonferroni[42] corrections were performed to adjust significance levels for multiple comparisons.

combined approach was significantly better than the RNFL-only or CPD-only approaches at 23 VF locations (16 after Holm–Bonferroni), largely in the superior and nasal regions of the VF. These results suggest that the combination of RNFL and vascular parameters may be advantageous for the study of focal structure–function associations with VF sensitivities in early glaucoma.

To the best of our knowledge, no prior studies have evaluated the structure–function relationship in glaucoma using a combination of RNFL and vascular parameters in a focal approach. Previous studies have mainly focused on the investigation of structure–function models based on either structural thickness[28,34,43,44] or vascular parameters.[14,16,17,21,22,30,33] Structural parameters based on RNFL measurements demonstrated a residual floor effect at greater severities ranging from −10 dB[16,41,44] to −14 dB,[32,38] in which increasing VF losses were not associated with corresponding thinning of the RNFL. In comparison, with vascular parameters from OCTA, such residual floor effects are less pronounced[16,38] or occur at greater VF losses compared with RNFL parameters. These studies have focused on subjects with higher glaucoma severities, but there are limited data on comparable structure–function studies in subjects with earlier glaucoma. In a recent study with 10-2 and 24-2 visual fields and with OCT scans from the macula and the optic disc, Hood and co-workers[45] demonstrated good agreement between abnormal structural thickness and functional regions in a cohort of eyes with early glaucoma. In another study of eyes with early glaucoma by Mansoori and co-workers,[18] significant correlations were demonstrated in the inferotemporal and superotemporal regions between structural thickness and vascular measures. However, these observations were not evaluated against VF losses. In our study, structure–function modeling using RNFL thickness or vascular measures was similar. The improved modeling of VF loss with both RNFL and vascular parameters is supported by studies that have postulated an autoregulatory mechanism in the ocular blood flow during glaucoma in which loss of retinal ganglion cells, which may in itself be attributed to vascular dysfunctionalities,[8,9] results in decreased regional demand and reductions in capillary perfusion.[5,46]

The improved modeling using the combined RNFL–CPD approach indicates that both structural thickness and vascular changes can be helpful in the structure–function relationship. Our findings are supported by a study of 47 eyes with mild to moderate glaucoma (VFMD, −4.39 ± 4.14 dB) by Hwang and co-workers.[24] The study evaluated the relationships among VF, RNFL structure, and blood flow measurements using Doppler OCT and showed that blood flow and structural measurements were independent but were only partial predictors of VF loss based on a multivariate regression analysis. Locations in which the combined model was not found to be better were largely located in the inferotemporal region, for which neither the RNFL nor the CPD models resulted in significant correlations. This could be understood from the patterns of early glaucomatous loss where the inferior and temporal VF regions are affected to a lesser extent compared with the superior hemifield.

The structure–function relationship was evaluated separately for each individual VF test point based on the functional losses from VF testing. Unlike other approaches that group a number of VF test points and provide a summary value based on an aggregate value of the VF losses in the group, our focal approach worked directly on the losses at each test point. This allowed a more specific modeling of localized VF sensitivity with the associated local RNFL and vascular parameters, which has been suggested as a better approach for evaluation of the structure–function relationship.[44] Although they are modeled individually, it is interesting to note from Figure 3 that the spatial locations of VF points with significant correlations are located largely in the superior nasal region of the VF. This is consistent with trends in the development of early glaucoma, in which the superior VF has been shown to be most susceptible to VF loss.[47] The focal modeling results are also consistent with other studies that have described the superotemporal and inferotemporal regions[17,41] as areas of increased vulnerability to glaucomatous losses.

Investigative Ophthalmology & Visual Science

There are several limitations to this study. Only parameters from optic disc scans were used. Including characteristics from macular scans such as ganglion cell layer thickness and retinal capillary density can be useful for defining the structure–function relationship.[17,38,41] Structural measurements of the RNFL currently include both neuronal components and vascular components, and isolation of the neuronal components may provide a more targeted consideration for structure–function modeling.[48] Vascular parameters were obtained from OCTA, which does not provide an actual quantification of blood flow but does provide a visualization of ocular perfusion, which has been shown to be a close approximation of vascular characteristics.[12] Assessments of structure–function relationships were limited to linear mixed models,[41] and other approaches were not considered. Only subjects from a single ethnicity were included in this study.[49] Due to the cross-sectional nature of the study, causal relationships among RNFL changes, vascular changes, and VF losses could not be determined. VF test–retest variability, particularly in focal regions of poorer sensitivities,[50] can also limit the reliability of the results. Further studies with repeated VFs incorporating data from other ethnicities are needed to evaluate the generalizability of the findings presented in this study.

In conclusion, the current study showed that the combination of RNFL measurements from OCT and vascular parameters from OCTA led to better focal structure–function relationships in eyes with early POAG. The results suggest that considering both focal structural thickness and vascular characteristics could improve modeling of VF defects, and further studies are needed to evaluate the generalizability of these findings.

Acknowledgments

Supported by grants from the National Medical Research Council (CG/C010A/2017_SERI, OFIRG/0048/2017, OFLCG/004c/2018, TA/MOH-000249-00/2018, and MOH-OFIRG20nov-0014); National Research Foundation Singapore (NRF2019-THE002-0006 and NRF-CRP24-2020-0001); A*STAR (A20H4-b0141); the Singapore Eye Research Institute & Nanyang Technological University (SERI-NTU Advanced Ocular Engineering [STANCE] Program); the Duke-NUS Medical School (Duke-NUS-KP(Coll)/2018/0009A); and the SERI-Lee Foundation (LF1019-1). The sponsors or funding organizations had no role in the design or conduct of this research.

Disclosure: **D. Wong**, None; **J. Chua**, None; **B. Tan**, None; **X. Yao**, None; **R. Chong**, None; **C.C.A. Sng**, None; **R. Husain**, None; **T. Aung**, None; **D. Garway-Heath**, None; **L. Schmetterer**, None

References

1. Brusini P, Johnson CA. Staging functional damage in glaucoma: review of different classification methods. *Surv Ophthalmol*. 2007;52:156–179.
2. Medeiros FA, Zangwill LM, Bowd C, Vessani RM, Susanna R, Weinreb RN. Evaluation of retinal nerve fiber layer, optic nerve head, and macular thickness measurements for glaucoma detection using optical coherence tomography. *Am J Ophthalmol*. 2005;139:44–55.
3. Wong D, Chua J, Baskaran M, et al. Factors affecting the diagnostic performance of circumpapillary retinal nerve fibre layer measurement in glaucoma. *Br J Ophthalmol*. 2021;105:397–402.
4. Flammer J, Orgul S, Costa VP, et al. The impact of ocular blood flow in glaucoma. *Prog Retin Eye Res*. 2002;21:359–393.
5. Yoshioka T, Song Y, Kawai M, et al. Retinal blood flow reduction in normal-tension glaucoma with single-hemifield damage by Doppler optical coherence tomography. *Br J Ophthalmol*. 2021;105:124–130.
6. Kiyota N, Shiga Y, Omodaka K, Pak K, Nakazawa T. Time-course changes in optic nerve head blood flow and retinal nerve fiber layer thickness in eyes with open-angle glaucoma. *Ophthalmology*. 2021;128:663–671.
7. Abegão Pinto L, Willekens K, Van Keer K, et al. Ocular blood flow in glaucoma - the Leuven Eye Study. *Acta Ophthalmol*. 2016;94:592–598.
8. Schmidl D, Garhofer G, Schmetterer L. The complex interaction between ocular perfusion pressure and ocular blood flow - relevance for glaucoma. *Exp Eye Res*. 2011;93:141–155.
9. Cherecheanu AP, Garhofer G, Schmidl D, Werkmeister R, Schmetterer L. Ocular perfusion pressure and ocular blood flow in glaucoma. *Curr Opin Pharmacol*. 2013;13:36–42.
10. Kashani AH, Chen C-L, Gahm JK, et al. Optical coherence tomography angiography: a comprehensive review of current methods and clinical applications. *Prog Retin Eye Res*. 2017;60:66–100.
11. Jia Y, Tan O, Tokayer J, et al. Split-spectrum amplitude-decorrelation angiography with optical coherence tomography. *Opt Express*. 2012;20:4710–4725.
12. Yao X, Ke M, Ho Y, et al. Comparison of retinal vessel diameter measurements from swept-source OCT angiography and adaptive optics ophthalmoscope. *Br J Ophthalmol*. 2021;105:426–431.
13. Yarmohammadi A, Zangwill LM, Diniz-Filho A, et al. Optical coherence tomography angiography vessel density in healthy, glaucoma suspect, and glaucoma eyes. *Invest Ophthalmol Vis Sci*. 2016;57:OCT451–OCT459.
14. Sakaguchi K, Higashide T, Udagawa S, Ohkubo S, Sugiyama K. Comparison of sectoral structure-function relationships in glaucoma: vessel density versus thickness in the peripapillary retinal nerve fiber layer. *Invest Ophthalmol Vis Sci*. 2017;58:5251–5262.
15. Rao HL, Pradhan ZS, Weinreb RN, et al. Vessel density and structural measurements of optical coherence tomography in primary angle closure and primary angle closure glaucoma. *Am J Ophthalmol*. 2017;177:106–115.
16. Wong D, Chua J, Lin E, et al. Focal structure-function relationships in primary open-angle glaucoma using OCT and OCT-A measurements. *Invest Ophthalmol Vis Sci*. 2020;61:33.
17. Shin JW, Lee J, Kwon J, Choi J, Kook MS. Regional vascular density-visual field sensitivity relationship in glaucoma according to disease severity. *Br J Ophthalmol*. 2017;101:1666–1672.
18. Mansoori T, Sivaswamy J, Gamalapati JS, Balakrishna N. Radial peripapillary capillary density measurement using optical coherence tomography angiography in early glaucoma. *J Glaucoma*. 2017;26:438–443.
19. Akil H, Huang AS, Francis BA, Sadda SR, Chopra V. Retinal vessel density from optical coherence tomography angiography to differentiate early glaucoma, pre-perimetric glaucoma and normal eyes. *PLoS One*. 2017;12:e0170476.
20. Chen CL, Bojikian KD, Wen JC, et al. Peripapillary retinal nerve fiber layer vascular microcirculation in eyes with glaucoma and single-hemifield visual field loss. *JAMA Ophthalmol*. 2017;135:461–468.
21. Chen C-L, Zhang A, Bojikian KD, et al. Peripapillary retinal nerve fiber layer vascular microcirculation in glaucoma using optical coherence tomography-based microangiography. *Invest Ophthalmol Vis Sci*. 2016;57:OCT475–OCT485.

22. Akagi T, Iida Y, Nakanishi H, et al. Microvascular density in glaucomatous eyes with hemifield visual field defects: an optical coherence tomography angiography study. *Am J Ophthalmol*. 2016;168:237–249.
23. Yarmohammadi A, Zangwill LM, Diniz-Filho A, et al. Relationship between optical coherence tomography angiography vessel density and severity of visual field loss in glaucoma. *Ophthalmology*. 2016;123:2498–2508.
24. Hwang JC, Konduru R, Zhang X, et al. Relationship among visual field, blood flow, and neural structure measurements in glaucoma. *Invest Ophthalmol Vis Sci*. 2012;53:3020–3026.
25. Calzetti G, Mursch-Edlmayr AS, Bata AM, et al. Measuring optic nerve head perfusion to monitor glaucoma: a study on structure-function relationships using laser speckle flowgraphy [published online ahead of print April 20, 2021]. *Acta Ophthalmol*, https://doi.org/10.1111/aos.14862.
26. Malik R, Swanson WH, DF Garway-Heath. 'Structure-function relationship' in glaucoma: past thinking and current concepts. *Clin Exp Ophthalmol*. 2012;40:369–380.
27. Medeiros FA, Zangwill LM, Bowd C, Mansouri K, Weinreb RN. The structure and function relationship in glaucoma: implications for detection of progression and measurement of rates of change. *Invest Ophthalmol Vis Sci*. 2012;53:6939–6946.
28. Harwerth RS, Wheat JL, Fredette MJ, Anderson DR. Linking structure and function in glaucoma. *Prog Retin Eye Res*. 2010;29:249–271.
29. Hoffmann EM, Medeiros FA, Sample PA, et al. Relationship between patterns of visual field loss and retinal nerve fiber layer thickness measurements. *Am J Ophthalmol*. 2006;141:463–471.
30. Yarmohammadi A, Zangwill LM, Diniz-Filho A, et al. Peripapillary and macular vessel density in patients with glaucoma and single-hemifield visual field defect. *Ophthalmology*. 2017;124:709–719.
31. Kadziauskienė A, Chua J, Baskaran M, et al. Association between structure-function characteristics and visual field outcomes in glaucoma subjects with intraocular pressure reduction after trabeculectomy. *Journal of Glaucoma*. 2020;29:648–655.
32. Mwanza JC, Budenz DL, Warren JL, et al. Retinal nerve fibre layer thickness floor and corresponding functional loss in glaucoma. *Br J Ophthalmol*. 2015;99:732–737.
33. Rao HL, Pradhan ZS, Weinreb RN, et al. Relationship of optic nerve structure and function to peripapillary vessel density measurements of optical coherence tomography angiography in glaucoma. *J Glaucoma*. 2017;26:548–554.
34. Wollstein G, Kagemann L, Bilonick RA, et al. Retinal nerve fibre layer and visual function loss in glaucoma: the tipping point. *Br J Ophthalmol*. 2012;96:47–52.
35. Garway-Heath DF, Poinoosawmy D, Fitzke FW, Hitchings RA. Mapping the visual field to the optic disc in normal tension glaucoma eyes. *Ophthalmology*. 2000;107:1809–1815.
36. Jansonius NM, Nevalainen J, Selig B, et al. A mathematical description of nerve fiber bundle trajectories and their variability in the human retina. *Vision Res*. 2009;49:2157–2163.
37. Jansonius NM, Schiefer J, Nevalainen J, Paetzold J, Schiefer U. A mathematical model for describing the retinal nerve fiber bundle trajectories in the human eye: average course, variability, and influence of refraction, optic disc size and optic disc position. *Exp Eye Res*. 2012;105:70–78.
38. Moghimi S, Bowd C, Zangwill LM, et al. Measurement floors and dynamic ranges of OCT and OCT angiography in glaucoma. *Ophthalmology*. 2019;126:980–988.
39. Mills RP, Budenz DL, Lee PP, et al. Categorizing the stage of glaucoma from pre-diagnosis to end-stage disease. *Am J Ophthalmol*. 2006;141:24–30.
40. Wang RK, An L, Francis P, Wilson DJ. Depth-resolved imaging of capillary networks in retina and choroid using ultrahigh sensitive optical microangiography. *Opt Lett*. 2010;35:1467–1469.
41. Hood DC, Kardon RH. A framework for comparing structural and functional measures of glaucomatous damage. *Prog Retin Eye Res*. 2007;26:688–710.
42. Holm S. A simple sequentially rejective multiple test procedure. *Scand J Stat*. 1979;6:65–70.
43. Mwanza JC, Kim HY, Budenz DL, et al. Residual and dynamic range of retinal nerve fiber layer thickness in glaucoma: comparison of three OCT platforms. *Invest Ophthalmol Vis Sci*. 2015;56:6344–6351.
44. Hood DC, Anderson SC, Wall M, Kardon RH. Structure versus function in glaucoma: an application of a linear model. *Invest Ophthalmol Vis Sci*. 2007;48:3662–3668.
45. Hood DC, Tsamis E, Bommakanti NK, et al. Structure-function agreement is better than commonly thought in eyes with early glaucoma. *Invest Ophthalmol Vis Sci*. 2019;60:4241–4248.
46. Sehi M, Goharian I, Konduru R, et al. Retinal blood flow in glaucomatous eyes with single-hemifield damage. *Ophthalmology*. 2014;121:750–758.
47. Gazzard G, Foster PJ, Viswanathan AC, et al. The severity and spatial distribution of visual field defects in primary glaucoma: a comparison of primary open-angle glaucoma and primary angle-closure glaucoma. *Arch Ophthalmol*. 2002;120:1636–1643.
48. Yow AP, Tan B, Chua J, Husain R, Schmetterer L, Wong D. Segregation of neuronal-vascular components in retinal nerve fiber layer for thickness measurement using OCT and OCT angiography. *Biomed Opt Exp*. 2021;12:3228–3240.
49. Chua J, Schwarzhans F, Nguyen DQ, et al. Compensation of retinal nerve fibre layer thickness as assessed using optical coherence tomography based on anatomical confounders. *Br J Ophthalmol*. 2020;104:282–290.
50. Artes PH, Iwase A, Ohno Y, Kitazawa Y, Chauhan BC. Properties of perimetric threshold estimates from full threshold, SITA standard, and SITA fast strategies. *Invest Ophthalmol Vis Sci*. 2002;43:2654–2659.

Investigative Ophthalmology & Visual Science